ELSEVIER

Inner-shell excitation of gas phase carbonates and α,γ-dicarbonyl compounds

Robert Lessard, Jérôme Cuny [1], Glyn Cooper, Adam P. Hitchcock *

Department of Chemistry, McMaster University, Hamilton, Ont., Canada L8S 4M1

Abstract

The inner-shell (C 1s, N 1s, O 1s) excitation spectra of dimethoxymethanone, diphenoxymethanone, and a series of α,γ-dicarbonyl compounds – 2,4-pentanedione, *N*-acetylacetamide, malonamide, acetyl anhydride, dimethyl malonate, diethyl malonate, 2-imidodicarbonic diamide, di-*t*-butyl iminodicarboxylate and dimethyldicarbonate – have been recorded in the gas phase with inner shell electron energy loss spectroscopy in the scattering regime dominated by electric dipole transitions. All spectra are presented on absolute oscillator strength intensity scales. They are interpreted with the aid of chemical series systematics and with the help of *ab initio* calculations. As found in a recent study of the X-ray absorption spectra of condensed carbonyl compounds [S.G. Urquhart, H. Ade, J. Phys. Chem. B 106 (2002) 8531], there is a very systematic correlation of the C 1s → $\pi^*_{C=O}$ transition energy and the relative oxidation at the carbonyl carbon, as expressed by a suitable oxidation index such as the sum of the atomic numbers or Pauling electronegativities of the elements bonded to the carbonyl carbon. Although the calculations clearly show there is delocalization between the two carbonyl groups, this had no detectible influence on the inner shell spectra. The absence of signals associated with π^* delocalization is explained in terms of core hole localization and symmetry effects.
© 2006 Elsevier B.V. All rights reserved.

Keywords: Inner shell excitation; Carbonates; Dicarbonyl compounds; Localized core hole

1. Introduction

Inner-shell excitation can be studied by either inelastic electron scattering (ISEELS) [1,2] or Near Edge X-ray absorption fine structure (NEXAFS) [3–6]. Recently there has been considerable activity in developing inner-shell excitation spectroscopy for high spatial resolution analysis, either by NEXAFS X-ray microscopy [7–12] or ISE-ELS in a transmission electron microscope [13,14]. When implemented at high spatial resolution, inner-shell excitation spectroscopy is a useful tool for the microanalysis of many types of materials. However for maximum analytical utility it is important to have spectra of com-

pounds of known structure for fingerprint purposes. In most cases, it is also very helpful to have detailed spectroscopic assignments. These can be derived from comparisons of series of closely related chemical species, aided by the results of high-quality quantum chemical calculations [15,16]. Here we report a systematic experimental and computational study of the inner shell spectra of two organic carbonate compounds (dimethoxymethanone and diphenoxymethanone) and nine α,γ-dicarbonyl compounds – 2,4-pentanedione, *N*-acetylacetamide, malonamide, acetyl anhydride, dimethyl malonate, diethyl malonate, 2-imidodicarbonic diamide, di-*t*-butyl iminodicarboxylate and dimethyldicarbonate. Scheme 1 displays the molecular structure of these species, organized in a way that emphasizes the systematic changes in the oxidation state of the carbonyl carbon atom. The letter codes shown are used to refer to the molecules in this paper. We use two different semi-quantitative parameters as

---

* Corresponding author. Tel.: +1 905 525 9104; fax: +1 905 521 2773.
E-mail address: aph@mcmaster.ca (A.P. Hitchcock).
[1] Visiting student from Ecole Nationale Supérieure de Chimie de Rennes, France.
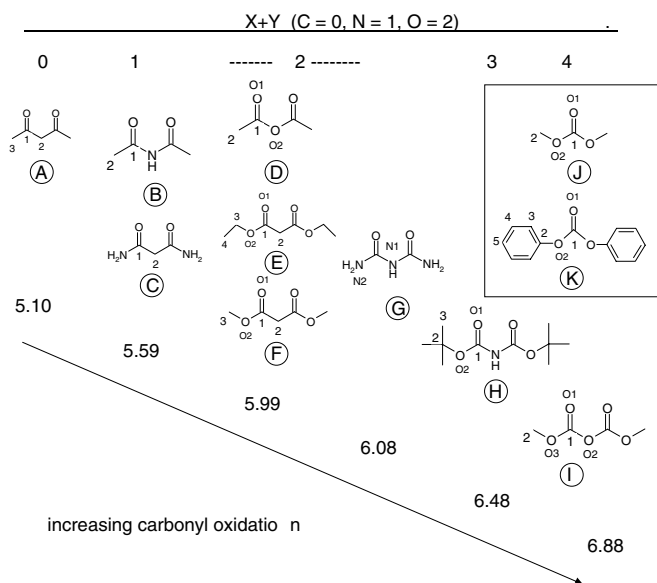
Scheme 1. Molecular structure of the α,γ-dicarbonyl and carbonate compounds studied: 2,4-pentanedione (A), N-acetylacetamide (B), malonamide (C), acetyl anhydride (D), dimethyl malonate (E), diethyl malonate (F), 2-imidodicarbonic diamide (G), di-t-butyl iminodicarboxylate (H), dimethyldicarbonate (I), dimethoxymethanone (J) and diphenoxymethanone (K). The numbers at the top are the 'oxidation index', the sum of numbers characteristic of the two atoms bonded to the carbonyl (C = 0, N = 1, O = 2). The numbers at the bottom are the sum of the Pauling electronegativities [17] of the two atoms bonded to the carbonyl.

correlators for the changes in the oxidation state of the carbonyl carbon atom. One, which we call the oxidation index, is the sum of numbers for the 2 atoms bonded to the carbonyl carbon, where C is assigned 0, N is assigned 1 and O is assigned 2. (For example, the carbonyl in 2-imidodicarbonic diamide (G) is bonded to two N atoms so its oxidation index is 2.) The other is the sum of the Pauling electronegativities [17] of the two atoms bonded to the carbonyl (for 2-imidodicarbonic diamide, this is $2 \times 3.04 = 6.08$).

The major focus of this study is the systematic variation of the energy and intensity of the $1s \rightarrow \pi^*_{C=O}$ transition as a function of the local structure around the carbonyl group. A similar combined experimental–computational study by Urquhart and Ade [18] of a series of condensed phase carbonyl compounds found a remarkably systematic variation of the $1s \rightarrow \pi^*_{C=O}$ transition energy as a function of the relative oxidation level of the carbonyl carbon, as determined by the elements adjacent to the carbonyl carbon. Aside from the two carbonates, all of the molecules studied in this work contain two carbonyl groups linked either by a —CH₂, —NH— or —O—; thus, we label the generic structure as Y(CO)X(CO)Y. A secondary theme of this study is to search for evidence of electronic delocalization between the two carbonyl groups. A further motivation for the study is to provide an expanded data base to assist interpretation of the inner shell spectra of polymer species containing carbonyl groups, which have been the subjects of earlier investigations [19–23].

This paper is organized as follows. After describing the experimental procedures and GSCF3 ab initio computational methods [15,16], the experimental spectra are presented and their main features interpreted based on systematic trends. Selected computational results are then presented to elaborate the spectral interpretation. In the discussion, the systematics of the energy shifts as a function of the oxidation index are analyzed. Extensive details of the computational results are presented as supplementary material.

2. Experimental

2.1. Materials

All compounds were obtained commercially from Sigma–Aldrich and were reported to have purities of 97% or greater: The solid materials were pumped to remove volatile impurities and then the vapor over the solid was introduced into the gas cell of the spectrometer using a method appropriate to its volatility.

2.2. Inner shell electron energy loss spectrometer

The apparatus and procedures of ISEELS have been described in detail elsewhere [1]. A final electron energy of 2.5 keV was used so that the spectra are dominated by electric dipole transitions and thus are very close to the corresponding NEXAFS spectra. The energy resolution was typically 0.7 eV fwhm, with the region of sharp structure at the C 1s onset recorded with a resolution of ∼0.55 eV fwhm, which is achieved by reducing the incident electron beam current to a few microamps in order to reduce space charge broadening. The spectra were obtained from the vapor above a solid sample, either introduced through a leak valve, or by placing ∼0.1 g in a metal tube directly attached to the collision cell, in order to achieve a local pressure of the order of 1×10^{-5} torr. The energy scale was calibrated by recording simultaneously the spectrum of the unknown and that of CO, N_2, O_2 [24,25] or CO_2 [26], as outlined in the footnotes to the tables.

2.3. Ab initio calculations

To aid spectral assignment, ab initio calculations of the C $1s \rightarrow \pi^*_{C=O}$ core excitation transitions were carried out using Kosugi's GSCF3 package [15]. Significant alterations in the electronic structure due to relaxation in core excited states make these high level calculations necessary in order to reliably assign inner shell spectra [27,28]. These calculations are based on the improved virtual orbital approximation (IVO) which explicitly takes into account the core hole in the Hartree–Fock approximation [29,30]. They are highly optimised for calculation of core excited states. A separate calculation is performed for each core excited atom. The difference in the total energy between the core ionised and ground state energies gives the core ionisation

potential (IP) with a typical accuracy of ≈1 eV. The absolute accuracy of the predicted ionisation potential is dependent on the size of the basis set. However, the term values of the core states ($TV = IP - E$) obtained in the IVO approximation are less dependent on the size of the basis set. This method of calculation treats the molecule as if it had a localized core hole. It is well known [31] that this is the most computationally efficient way for reproducing the strong core hole relaxation effects. Strictly speaking the solutions for sites with multiple symmetry-equivalent atoms (i.e. the C 1s and O 1s of the dicarbonyls) should be re-symmetrized to represent symmetry correct solutions, as has been done in other applications of GSCF3 [32], since the system will undergo symmetry breaking and have an actual localized core hole only if there is excitation of an appropriate non-totally symmetric vibrational mode [33,34]. However, we expect little change in the computed spectra to result from this exercise, as was found in earlier work [32].

The molecular geometries were generated by *ab initio* geometry optimization at the 4-21G level using the program GAMESS [35] or at the 3-21G* level using SPARTAN [36]. Identical basis sets (Huzinaga et al. [37]) were used for all GSCF3 *ab initio* calculations. Those used were: for the core excited atom, a 411121 3111 expansion of the 736 HTS8X basis set plus one diffuse polarization function; for other heavy atoms, a 621 41 expansion of the 635 HTS6X basis set; for the H atoms a 41 expansion of the 5 HTS2X basis set. The input files used for the calculations are provided in the supplementary materials.

3. Results and discussion

3.1. C 1s spectra

Fig. 1 presents the C 1s spectra of the two carbonate and nine α,γ-dicarbonyl compounds, background subtracted and placed on an absolute oscillator strength scale using methods described previously [2]. In this plot the intensity scale is the oscillator strength for the full molecule rather than the per-C atom presentation that has been used in other publications. The sequence of the molecules was chosen in order of increasing energy of the C 1s → $\pi^*_{C=O}$ transition. The energies and proposed assignments of spectral features are listed in Tables 1–3. All spectra are reported for the first time to the best of our knowledge. The experimental data (both raw ISEELS and after conversion to optical oscillator strength) are available in the supplemental materials and also available from http://unicorn.mcmaster.ca/corex/cedb-title.html. The spectra of all species except diphenoxymethanone are dominated by the C 1s → $\pi^*_{C=O}$ transition. In diphenoxymethanone, while the $\pi^*_{C=O}$ peak is readily detected, the spectrum is dominated by the C 1s → $\pi^*_{C=C}$ transition at the 12 ring carbon atoms. The shifts in the energy and intensity of the $\pi^*_{C=O}$ peak are discussed in detail below. Other C 1s spectral features are associated with 1s → σ^*_{C-H}, 1s → σ^*_{C-C} and
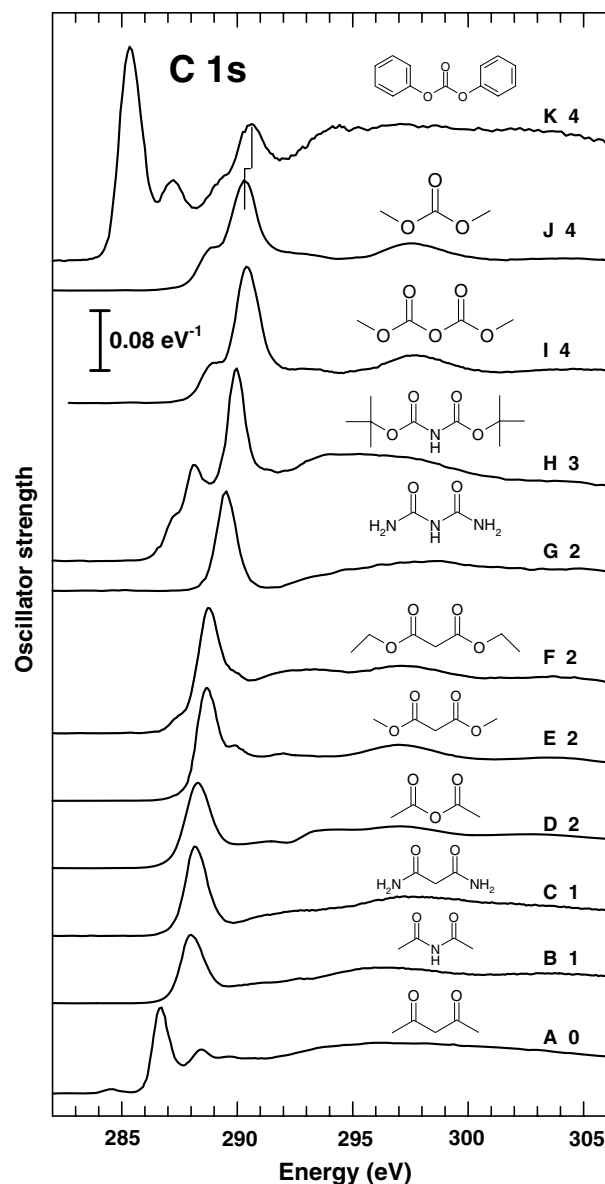

Fig. 1. Oscillator strengths for C 1s excitation of 2,4-pentanedione (A), *N*-acetylacetamide (B), malonamide (C), acetyl anhydride (D), dimethyl malonate (E), diethyl malonate (F), 2-imidodicarbonic diamide (G), di-*t*-butyl iminodicarboxylate (H), dimethyldicarbonate (I), dimethoxymethanone (J) and diphenoxymethanone (K), derived from inner shell electron energy loss (ISEELS) spectra recorded in the electric dipole regime (2.5 keV final electron energy, 2° scattering angle). The pre-C 1s signal has been extrapolated through the energy range plotted and subtracted. The intensity scale is absolute on a per molecule basis. Offsets are used for clarity. The molecular structure, molecule letter code, and the oxidation index are indicated for each species.

1s → $\sigma^*_{C=O}$ transitions, as outlined in the tables of assignments.

3.2. O 1s spectra

Fig. 2 presents the O 1s spectra of the two carbonate and nine α,γ-dicarbonyl compounds, background subtracted and placed on absolute oscillator strength scale (total for the full molecule). The sequence of the molecules is the

Table 1
Energies (±0.1 eV) and proposed assignments of features in the C 1s spectra of species with oxidation index of 0 (A) and 1 (B, C)

Species (ox. index)			Assignment		
A (0)	B (1)	C (1)	CH$_3$	CH$_2$	C=O
284.5	–	–	Impurity		
286.65(8)[a]	287.97(5)[a]	288.21(5)[a]			π^*
288.4			σ^*_{C-H}		
289.7	291.1	291.3 (sh)	Ryd	Ryd	
–	–	292.6		σ^*_{C-C}	
294(1) sh	292.7	–	σ^*_{C-C}		
296 br	–	–		σ^*_{C-C}	
–	296.4	297.6			σ^*_{C-N}
304 (sh)	303.6	301.6			$\sigma^*_{C=O}$

[a] Calibration: A: −4.09(3) eV relative to the π^* transition in CO$_2$ (290.74(6) [26]). B, C: 0.57(5), 0.81(3) eV relative to the π^* transition in CO (287.40(2) [24,25]) respectively.

same as that in Fig. 1. The energies and proposed assignments of spectral features are listed in Table 4. The spectra of all species are dominated by the O 1s(C=O) → $\pi^*_{C=O}$ transition. The shifts in the energy and intensity of the $\pi^*_{C=O}$ peak are discussed in detail below. In the seven compounds containing ester groups (D, E, F, H, I, J, K), there is a second π^* feature attributed to O1s(C—O) → $\pi^*_{C=O}$ transitions, arising from partial delocalization of the $\pi^*_{C=O}$ orbital onto the adjacent O atom. In the continuum there are features are associated with O 1s(C—O) → σ^*_{C-O} and O 1s(C=O) → $\sigma^*_{C=O}$ transitions, as outlined in the tables of assignments. The O 1s spectrum of diphenoxymethanone (K) is particularly noteworthy since the location of both the O 1s(C=O) → $\pi^*_{C=O}$ and O 1s(C—O) → $\pi^*_{C=O}$ transitions are displaced relative to those in dimethoxymethanone (J) (and also dimethyldicarbonate (I)), with the carbonyl O 1s excitation being shifted downward by ∼1 eV and the ester O 1s excitation being shifted upward by ∼1 eV. Initially these shifts were attributed to delocalization associated with electronic interactions of the carbonyl $\pi^*_{C=O}$ orbitals and the phenyl ring $\pi^*_{C=C}$ orbitals. Surprisingly there are no corresponding shifts in the C 1s spectrum of K relative to that of J. Further discussion is given when presenting the computational results for these molecules.

Table 2
Energies (±0.1 eV) and proposed assignments of features in the C 1s spectra of species with oxidation index of 2 (D, E, F, G)

Species (ox. index)				Assignment		
D (2)	E (2)	F (2)	G (2)	CH$_3$	CH$_2$	C=O
–	–	287.5		Ryd		
288.34(5)[a]	288.70(8)[a]	288.76(8)[a]	289.52(4)[a]			π^*
291.4	289.9			σ^*_{C-H}		
	291.9	293.2 (sh)		Ryd	Ryd	
–		297.1			σ^*_{C-C}	
294.0		–	294.9			$\sigma^*_{C=O}$
297.0	297.0	–	298.4	σ^*_{C-C}		$\sigma^*_{C=O}$
302.6 (sh)	303.7	303.5	303.9			$\sigma^*_{C=O}$

[a] Calibration: D, E, G: 0.94(3), 1.30(7), 2.12(3) eV relative to the π^* transition in CO (287.40(2) [24,25]) respectively. F: −1.97(3) eV relative to the π^* transition in CO$_2$ (290.74(6) [26]).

Table 3
Energies (±0.1 eV) and proposed assignments of features in the C 1s spectra of species with oxidation index of 3 (H) and 4 (I, K, J)

Species (ox. index)				Assignment			
H (3)	I (4)	J (4)	K (4)	CH$_3$	CH$_2$	C=O	C=C (ring)
–	–		285.33(4)[a]				$1\pi^*_{ring}$
			287.2				$2\pi^*_{ring}$
287.3 (sh)				3s Ryd			
288.19	289.1	288.9	–	3p Ryd			
–	–		289.5				σ^*_{ring}
289.90(4)[a]	290.46(4)[a]	290.30(9)[a]	290.60			π^*	
291.3	–			σ^*_{C-C}			
–	–		292.7 (sh)				σ^*_{ring}
–	293.2	292.0		σ^*_{C-C}			
293.9 (sh)	–			σ^*_{C-C}			
			294.4				σ^*_{ring}
			297.1				σ^*_{ring}
296.5	297.7	297.6	–	σ^*_{C-C}		$\sigma^*_{C=O}$	
304.6 (sh)	304.7	304.6	303.2	σ^*_{C-C}		$\sigma^*_{C=O}$	

[a] Calibration: H, I, K: 2.50(3), 3.06(2), −2.07(3) eV relative to the π^* transition in CO (287.40(2) [24,25]) respectively. J: 4.63(5) eV relative to the π^* transition in C$_2$H$_2$ (285.67(8) [26]).
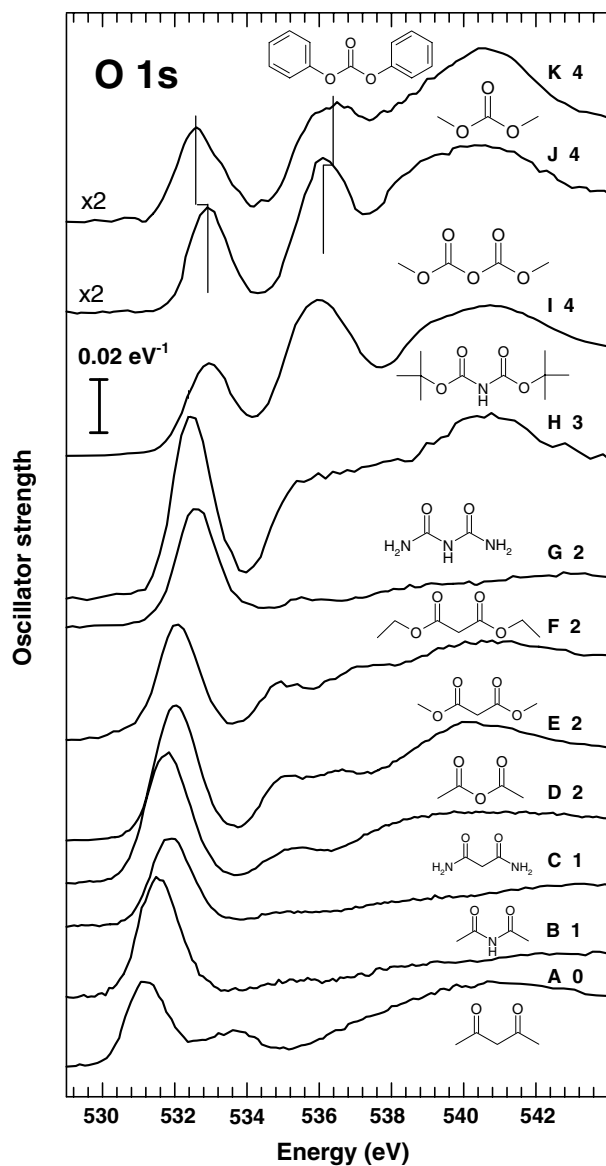
Fig. 2. Oscillator strengths for O 1s excitation of 2,4-pentanedione (A), *N*-acetylacetamide (B), malonamide (C), acetyl anhydride (D), dimethyl malonate (E), diethyl malonate (F), 2-imidodicarbonic diamide (G), di-*t*-butyl iminodicarboxylate (H), dimethyldicarbonate (I), dimethoxy-methanone (J) and diphenoxymethanone (K), derived from inner shell electron energy loss (ISEELS) spectra recorded in the electric dipole regime. The pre-O1s signal has been extrapolated and subtracted. Offsets are used for clarity. The intensity is that for the full molecule, except for J and K, which have been multiplied by 2 to compensate for the lower number of carbonyls, and thus allow direct comparison of the π^* intensity.

3.3. N 1s spectra

Fig. 3 presents the N 1s spectra of the four species containing N atoms, *N*-acetylacetamide (B), di-*t*-butyl iminodicarboxylate (H), malonamide (C) and 2-imidodicarbonic diamide (G). The energies and proposed assignments of spectral features are listed in Table 5. Low lying sharp peaks are observed in the N 1s spectra of all four species. While there is very likely mainly Rydberg and N–H σ^* character to these peaks, there is also most likely a contribution from

N 1s $\rightarrow \pi^*_{C=O}$ transitions arising because of partial delocalization of the carbonyl $\pi^*_{C=O}$ orbitals onto the adjacent N atoms. Malonamide (C) and 2-imidodicarbonic diamide (G) exhibit an apparent "doublet" structure. Since these are the only two species with a primary amine group it is very likely that the lowest energy peak in both of these spectra arises from excitations at the primary amine site. Since it is in a less electropositive environment, the N 1s(NH$_2$) orbital will have a lower binding energy than the N1s(NH) site, giving rise to transitions at lower energies. The detailed assignments of the N 1s spectra are discussed in more detail in conjunction with the computational results in the next section.

3.4. Computational results

Ab initio calculations were carried out using the GSCF3 program to compute the inner shell spectra of 2,4-pentanedione (A), *N*-acetylacetamide (B), malonamide (C), acetyl anhydride (D), dimethyl malonate (E), diethyl malonate (F), 2-imidodicarbonic diamide (G), di-*t*-butyl iminodicarboxylate (H), dimethyldicarbonate (I), dimethoxymethanone (J) and diphenoxymethanone (K). For each species, calculations were carried out for excitation at each core edge and for all symmetry inequivalent sites. The calculated energies and oscillator strengths of the C 1s $\rightarrow \pi^*_{C=O}$ transitions in all 10 molecular species are summarized in Table 6 in comparison with the experimental energies and intensities. Tabulations and plots of the computational results relative to experimental data are given for each edge of each molecule in the supplementary material.

Fig. 4 is an example – the results from the GSCF3 calculation of the C 1s spectrum of 2,4-pentanedione. It presents the calculated spectrum of each chemically distinct site, a weighted sum of these, and the experimental spectrum. The simulated spectra are generated assuming peak widths of 1.2, 2.0, 4.0 and 8.0 eV for transitions involving upper levels with term values lower than −2.0, +2.0, +8.0 eV and above +8.0 eV, respectively. Also shown are sharp lines which correspond to each calculated transition, the heights of which represent the calculated intensities of the transitions. The scale for the computed C 1s spectrum of 2,4-pentanedione has been shifted by −3.1 eV in order to align the main C 1s $\rightarrow \pi^*_{C=O}$ transition with experiment. This shift, which is ~3 eV for the C 1s spectra of all species, is typical of GSCF3 with the IVO approximation. The computed and experimental spectra are in reasonably good agreement. The computed C 1s spectrum of 2,4-pentanedione is typical of the calculations for all species (see the supplementary material for similar plots for each core edge of all species). The high intensity of the first peak results from C 1s(C—O) $\rightarrow \pi^*_{C=O}$ transitions, while lower intensity features (weaker shoulders, etc) result from transitions at the CH$_2$ and CH$_3$ sites. This is because the π^* final orbital has a much higher density on the carbonyl carbon atoms than on the other sites, hence higher overlap leading to more intense transitions.

Table 4
Energies (±0.1 eV) and proposed assignments of features in the O 1s spectra of carbonates and α,γ-dicarbonyls

Species (ox. index)			Assignment
A (0)	B (1)	C (1)	C=O

4A. A, B, C

A (0)	B (1)	C (1)	Assignment C=O
531.17(0)[a]	531.56(9)[a]	531.89(9)[a]	π^*
533.6	535.4	535.3	$\sigma^*_{C=O}$
		538.8	$\sigma^*_{C=O}$
541.2	544.2	543.3	$\sigma^*_{C=O}$
		546.5	$\sigma^*_{C=O}$

Species (ox. index)				Assignment		
D (2)	E (2)	F (2)	G (2)	O–CH$_3$	C–O–C	C=O

4B. D, E, F, G

D (2)	E (2)	F (2)	G (2)	O–CH$_3$	C–O–C	C=O
531.85(1)[b]	532.05(2)[b]	532.1(1)[b]	532.61(9)[b]			π^*
535.4					σ^*_{C-O}	
	535.2	535.1		σ^*_{C-O}		
			535.5			$\sigma^*_{C=O}$
540.8					σ^*_{C-O}	
	536.6	537.3		σ^*_{C-O}		
	540.3	540.8		σ^*_{C-O}		
546.5	546.0	546.8	542.9			$\sigma^*_{C=O}$

Species (ox. index)				Assignment		
H (3)	I (4)	J (4)	K (4)	RO–(CO)	C–O–C	C=O

4C. H, I, J, K

H (3)	I (4)	J (4)	K (4)	RO–(CO)	C–O–C	C=O
532.47(0)[c]	532.9	532.95(12)[c]	532.68(8)[c]			π^*
535.5	536.0	536.2	536.5	σ^*_{C-O}		
538	–			σ^*_{C-O}		$\sigma^*_{C=O}$
–	539.1				σ^*_{C-O}	
540.7	540.61(9)[c]	540.3	540.6	σ^*_{C-O}		$\sigma^*_{C=O}$
–	548(1)	548				$\sigma^*_{C=O}$

[a] Calibration: A: −4.24(6) eV relative to the π^* transition in CO2 (535.40(8) [26]). B, C: −2.65(0), −2.32(3) eV relative to the π^* transition in CO (534.21(9) [24,25]) respectively.

[b] Calibration: D, E, G: −2.37(6), −2.17(7), −1.60 eV relative to the π^* transition in CO (534.21(9) [24,25]) respectively. F: −3.35(3) eV relative to the π^* transition in CO$_2$ (535.40(8) [26]).

[c] Calibration: H, I, K: −1.76(5), 6.40(2) eV relative to the π^* transition in CO (534.21(9) [24,25]) respectively. J: 2.10(4) eV relative to the π^* transition in O$_2$ (530.8 [25]). K: −2.72(1) eV relative to the π^* transition in CO$_2$ (535.40(8) [26]).

Fig. 5 demonstrates why only one main C 1s → $\pi^*_{C=O}$ transition is observed in the C 1s spectra of this group of molecules, despite the potential of multiple π^* peaks being formed due to delocalization splitting that is expected in all but two of the molecules (J and K) studied in the present work. As the top panel of Fig. 5 shows, the $\pi^*_{C=O}$ levels are split in the ground state molecule by ~0.5 eV, with complete delocalization of electron density across both C=O groups. However, when a C 1s core hole is generated on one of the C atoms, the $\pi^*_{C=O}$ levels are split much more, by ~4.0 eV, due to the presence of the core hole that is localized on the excited C atom. As well as this energy splitting, the core hole also localizes the electron density in each of the $\pi^*_{C=O}$ levels onto one C=O or the other. This localization of the upper π^* level, combined with the localized core hole, means that the transition to the lowest energy orbital will be the only one observed experimentally. There is effectively no electron density on the core-excited C atom in the higher energy $\pi^*_{C=O}$ orbital. Fig. 5 also shows computed $\pi^*_{C=O}$ energies and MO plots for the situation where the X atom linking the two C=O groups is N or O instead

of C (middle and bottom panels). Effectively the same phenomenon is observed, although when the linking atom is N or O there is slightly more delocalization in the excited states, but not enough to lead to observable intensity in the C 1s spectra of the C=O carbon atoms.

Strong effects of core hole localization have been observed previously in the inner shell spectra of a number of molecules. In particular, although delocalization in the ground state spreads the $\pi^*_{C=O}$ levels over several eV, the inner shell C 1s excitation spectra of the metal carbonyl species Fe(CO)$_5$ [38,39], Ni(CO)$_4$ [40] and the hexacarbonyls M(CO)$_6$ (M = Cr, Mo, W) [41] each exhibit only a single, narrow main C 1s → $\pi^*_{C=O}$ transition, which is clearly a single electronic state since vibrational fine structure was resolved [40,41]. The absence of multiple C 1s → $\pi^*_{C=O}$ transitions was attributed to strong distortion of the π^* manifold by the localized core hole, which effectively collapses the upper level of the transition onto the C=O ligand with the core hole. Although the localized C 1s → $\pi^*_{C=O}$ transition dominates the spectrum, very weak additional features were observed at a few eV higher

0.005 eV⁻¹

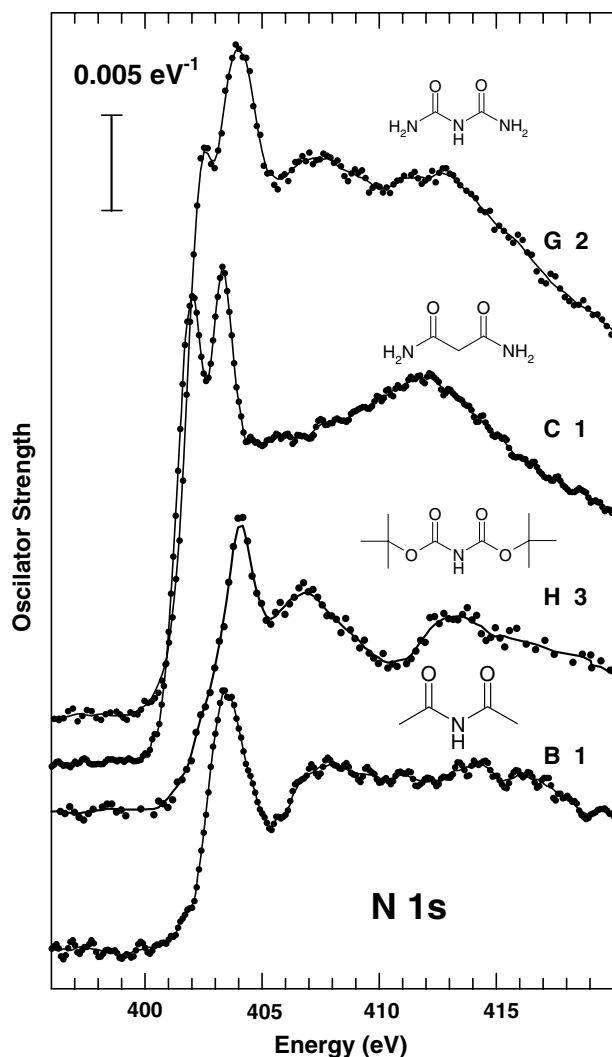**Oscilator Strength**

N 1s

400 405 410 415
Energy (eV)

Fig. 3. N 1s spectra of *N*-acetylacetamide (B), di-*t*-butyl iminodicarboxylate (H), malonamide (C) and 2-imidodicarbonic diamide (G derived from inner shell electron energy loss (ISEELS) spectra recorded in the electric dipole regime. The pre-N 1s signal has been extrapolated and subtracted. Points are the actual data, with the line showing a smoothed version of the data (9-point Savitsky–Golay smoothing, except in the region of the sharp structures). Offsets are used for clarity.

situations, the extensive delocalization through intermixing of the $\pi^*_{N=O}$ orbitals of the NO_2 groups and the $\pi^*_{C=C}$ orbitals of the phenyl rings in nitrobenzene and the nitroanilines was found to have a strong influence on their inner shell excitation spectra [42].

Fig. 6 explores the $X1s \rightarrow \pi^*_{C=O}$ inner shell excitation at the central atom in the $C=O–X–C=O$ grouping. The excited states must be symmetric when the core hole is created on this site. Therefore delocalization of the $\pi^*_{C=O}$ orbitals has to occur, and the large energy splitting seen as a result of core hole localization at one of the carbonyls is not observed. However, the lower energy of these two more closely spaced $\pi^*_{C=O}$ orbitals contains effectively zero electron density on the central atom due to its nodal structure, whereas the higher energy one contains appreciable density on the central atom which contains the core hole. Thus, a transition of significant intensity is calculated to occur from the core hole to this orbital. The net result is that only one π^* transition is observed in the excitation of the central atom. In the case of the computed C 1s spectrum of 2,4-pentanedione (Fig. 4), this transition is calculated to occur between the main C 1s $\rightarrow \pi^*_{C=O}$ transition and the ionization onset, and contributes to the intensity in this energy region. The smaller feature in the computed C $1s(CH_2)$ spectrum at low energy (slightly below the main C $1s \rightarrow \pi^*_{C=O}$ peak) is due to a mixed C–H $\sigma^*_{C-H}/\pi^*_{C=O}$ final orbital. It is of low intensity and has no simple representation. The features shown in Fig. 4 in the $C(CH_3)$ computed spectrum are very similar to those shown in the C $1s(CH_2)$ spectrum just discussed in that the lowest energy transition is weak and is calculated to arise from a final orbital of mixed C–H $\sigma^*_{C-H}/\pi^*_{C=O}$ character. There are identifiable transitions from the C $1s(CH_3)$ site to orbitals having significant $\pi^*_{C=O}$ character at energies between the main peak and the ionization onset, although in this case their density is concentrated towards the end of the molecule where the core hole is localized. The computational details discussed here and shown in Figs. 5 and 6 are generally applicable to the C 1s spectra of all the molecules of the $C=O–X–C=O$ series (see supplementary materials). There are some additional low energy features in the spectra of molecules with terminal CH_3 groups (such as H, I and J) which are calculated to be mainly C $1s \rightarrow$ C–H σ^*_{C-H} in character, although

energy. These were attributed to C $1s \rightarrow \pi^*_{delocalized}$ transitions. For $Fe(CO)_5$ this interpretation was supported by semi-empirical MO calculations [39]. In contrast to these

Table 5
Energies (± 0.1 eV) and proposed assignments of features in the N 1s spectra of α,γ-dicarbonyls

Species (ox. index)				Assignment	
B (1)	C (2)	G (2)	H (3)	$_2HN–C=O$	$(CO)–NH–(CO)$
–	401.7	402.6	–	σ^*_{N-H}	
	402.98(3)[a]	404.0[a]		σ^*_{N-H}, π^*	
402.85(2)[a]			404.07(3)[a]		σ^*_{N-H}, π^*
407.2		407.3	406.7		σ^*_{C-N}
				σ^*_{C-N}	
	411.6	412.6		σ^*_{C-N}	σ^*_{C-N}
413			413.3		σ^*_{C-N}
			417		σ^*_{C-N}

[a] Calibration: B, C, H: 1.75(0), 1.88(2), 2.97(2) eV relative to the π^* transition in N_2 (401.10(2) [24,25].), respectively. G was calibrated relative to its C $1s \rightarrow \pi^*_{C=O}$ transition, a difference of 114.5(1) eV.

Table 6
Comparison of experimental and calculated energies and intensities of C1s $\rightarrow \pi^*_{C=O}$ transitions

Code	OI[a]	Species	Experimental		Calculated	
			Energy (eV)	Intensity (/100)	Energy (eV)	Intensity (100)
A	0	2,4-pentanedione	286.65	9.8	289.80	12.8
–	0	Acetone[b]	286.81	–	289.60	–
B	1	N-acetylacetamide	287.97	11.5	291.05	12.4
C	1	Malonamide	288.21	14.6	291.31	13.2
D	2	Acetyl anhydride	288.34	13.4	291.52	13.2
E	2	Dimethyl malonate	288.70	12.9	291.68	13.7
F	2	Diethyl malonate	288.76	15.9	291.57	13.9
–	2	Phenyl urea[c]	289.51	–	292.18	–
G	2	2-imidodicarbonic diamide	289.52	14.5	292.54	13.5
H	3	Di-t-butyl iminodicarboxylate	289.90	12.3.	293.19	13.5
I	4	Dimethyldicarbonate	290.46	16.9	293.54	14.0
J	4	Dimethoxymethanone	290.30	19.2	293.46	14.7[d]
K	4	Diphenoxymethanone	290.60	14.2	293.76	13.5[de]

[a] OI = oxidation index (see text for definition).
[b] C 1s spectrum reported in [44].
[c] C 1s spectrum reported in [45].
[d] These values are multiplied by 2 to account for the fact there is only one carbonyl, whereas all the other species contain two carbonyl groups.
[e] The value for the planar geometry of K.

C 1s $\rightarrow$ Rydberg transitions are also expected at such energies. These latter features have no analogues in the O 1s spectra.

Fig. 7 presents the computed N 1s spectra of N-acetylacetamide (B) and malonamide (C), in comparison to the experimental spectra. The computed energy scale has been shifted by -1.3 and -1.7 eV for B and C respectively in order to align the main N 1s $\rightarrow \pi^*_{C=O}$ transition with experiment. In the discrete region most of the transitions are calculated to be σ^*_{N-H} in character. Indeed the most intense transitions are all of this character according to the calculations. As discussed above, N $1s \rightarrow$ Rydberg transitions are also expected to contribute to the spectra in the discrete region, although the theory (which cannot produce Rydberg transitions due to limitations of the basis set used) does an adequate job of reproducing the experimental results. The N 1s $\rightarrow \pi^*_{C=O}$ transitions that originate at NH$_2$ terminal groups (malonamide (Fig. 7) and 2-imidodicarbonic diamide) are calculated to be very weak, and show no delocalization over the two C=O groups. In contrast, the N 1s $\rightarrow \pi^*_{C=O}$ transitions that originate at the central N atoms in 2-imidodicarbonic diamide, N-acetylacetamide (Fig. 7) and di-t-butyliminodicarboxylate show significant intensity in the calculations, making significant contribution to the discrete spectral intensity in these molecules, and the final orbitals are delocalized over both C=O groups. Analogous to the C 1s spectra, only one of the possible N 1s (central) $\rightarrow \pi^*_{C=O}$ final orbitals is calculated to have appreciable intensity in each molecule due to symmetry considerations (nodal structure). See Fig. 6 (central panel) for details of the final orbitals in the N 1s (central) calculated spectrum of N-acetylacetamide. It is noteworthy that in 2-imidodicarbonic diamide, the N 1s $\rightarrow \pi^*_{C=O}$ transitions that originate from the terminal NH$_2$ groups are calculated to have a lower energy (by $\sim$3 eV) than those originating from the central NH group. This supports the

empirical assertion made in Section 3.3, that the N atoms in the NH$_2$ group are in a less electropositive environment, hence the N 1s(NH$_2$) orbitals will have a lower binding energy than those at the N 1s(NH) site, giving rise to transitions at lower energies.

The computed results for the O 1s spectra of the compounds studied in the present work are largely analogous to those for the C 1s and N 1s spectra discussed above, and are generally in reasonable agreement with experiment, once an energy shift to align the computed and experimental O 1s $\rightarrow \pi^*_{C=O}$ peaks is applied. For the O 1s excitation this is in the range of 1–2 eV (see supplementary material). In particular, the existence of O 1s $\rightarrow \pi^*_{C=O}$ transitions from both O($\underline{C}$=O) and O(C=O–$\underline{O}$) atoms is reproduced with the correct relative energies. Also, analogous to Fig. 4 (which shows C 1s excited final orbitals) the O 1s excitations that originate from O atoms in any other position in the molecules except for the position right between the two C=O groups in the α,γ-dicarbonyl compounds show final states that are localized almost exclusively on just one of the C=O groups (due to the core hole localization effect). Thus, only one O 1s $\rightarrow \pi^*_{C=O}$ transition is visible in the spectra. Only for dimethyl malonate (E) and dimethyldicarbonate (I), which have bridging O atoms, is delocalization visible in the final orbitals calculated in transitions from the central O atoms. Again, due to symmetry considerations, only one of these has spectral intensity (see bottom panel of Fig. 6 for the example of the O 1s(–O–) excited state of dimethyl malonate).

Fig. 8 presents computed O 1s spectra of diphenoxymethanone (K), in both planar and twisted conformations, in comparison to the experimental spectrum. Shifts of -1.5 eV for the planar and -2.1 eV for the twisted conformation were used to align the computed and experimental spectra. The energy minimized, twisted geometry (55° dihedral angle) is similar to that observed experimentally in the
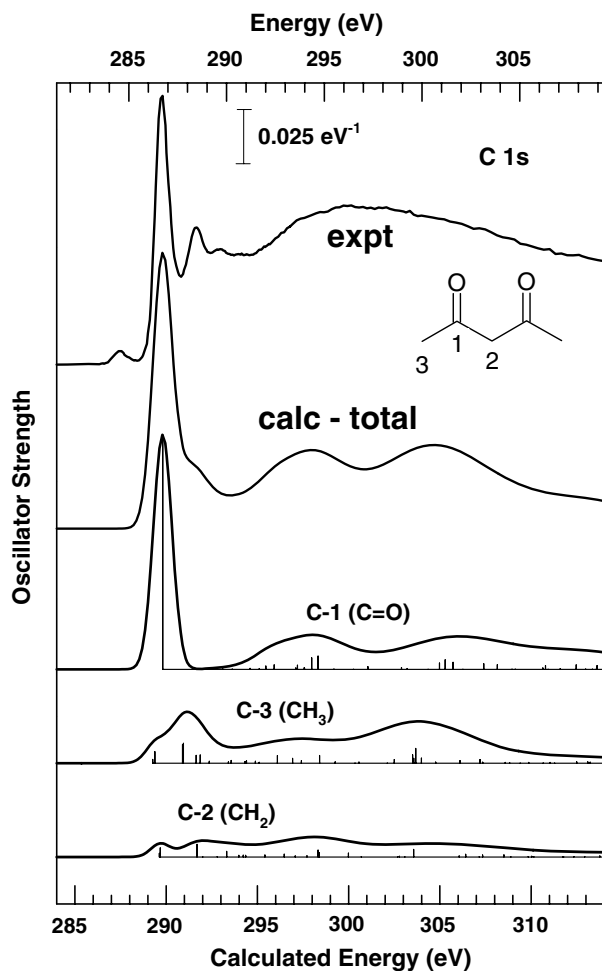
Fig. 4. Computational results for C 1s excitation of 2,4-pentanedione (A) compared to the experimental spectrum. The solid curves are the spectrum of each chemical site and the weighted sum, the thin lines indicate the individual transitions. The computed energy scale is offset by −3.1 eV relative to the experimental scale to align the C 1s → $\pi^*_{C=O}$ peaks. See text for further details of how the simulated spectra are derived from the computational results. Full details of the computations are given in the supplementary material.

solid [43]. We expect the gas phase geometry to be planar due to π interaction between the carbonate and the phenyl rings. As is evident in the figure, the calculated results are essentially identical for the two geometries, except for some very minor differences in the ~538–540 eV energy region – some additional intensity in this region is predicted for the planar geometry. Both sets of calculations indicate that delocalization of the $\pi^*_{C=O}$ final orbitals on to the phenyl rings essentially does not occur, even in the favorable planar geometry. The reason is localization of the O 1s core hole, which concentrates the final excited state on the central O–(C=O)–O grouping and prevents participation of the phenyl ring orbitals in this final excited state. Similar localization effects are also shown in the calculations of the C 1s spectrum of K for transitions that originate at the central C atom. For the C 1s spectrum, the transitions originating from the phenyl ring C atoms, which occur at lower energy, exhibit some degree of delocalization throughout the ring

structure, but not onto the central O–(C=O)–O grouping. This can be contrasted with the results obtained for nitrobenzene and the nitroanilines [42], where there is clear evidence for extensive final state delocalization of the substituent π* orbitals onto the phenyl rings. There, the calculations indicated that the N 1s(NH$_2$) → π* spectra of nitroanilines would change dramatically if the NH$_2$ group was twisted from planar to 90° out-of-plane [42]. This contrasts sharply with the case of K, where the spectra are insensitive to an analogous geometry change.

The C 1s and O 1s spectra of diphenoxymethanone (K) have interesting differences from that of dimethoxymethanone (J), as noted earlier. One may imagine the phenyl group in K to be electron withdrawing (or at least capable of more electron delocalization in the excited state) compared to the methyl group in J. Therefore, the C 1s and O 1s → $\pi^*_{C=O}$ transitions may be expected to be at higher energy in K than J. In fact, in the C 1s spectra (Fig. 1) this is the case – the C 1s → $\pi^*_{C=O}$ transition is 0.3 eV higher in energy in K than J. However, in the O 1s spectra, although the ester O atoms in K give rise to a O 1s → $\pi^*_{C=O}$ transition at slightly higher energy than the ester transition in J, the O 1s → $\pi^*_{C=O}$ transition originating at the carbonyl O atom in K is at a lower energy than the analogous transition in J. The computed spectra of the twisted and planar K geometries shown in Fig. 8 demonstrate that geometry is not a factor in this effect. Also, examination of the $\pi^*_{C=O}$ final state energies in K and J for both the carbonyl and ester excitations reveal no significant calculated differences between them. The energy separation calculated between the carbonyl and ester O 1s → $\pi^*_{C=O}$ transitions in K is also lower than observed experimentally. Therefore, it seems that the energy for formation of the O 1s hole on the C=O group of K is lower than that for formation of the O 1s hole in J, although it is not clear from our investigations as to why this might be so.

4. Discussion: chemical shift effects on the energy and intensity of the 1s → π^*_{CO} transitions

Fig. 9 plots the computed C 1s and O 1s spectra in the regions of the C1s(C=O) → π* and O 1s → π* transitions. Only the calculated 1s → π* transitions are plotted in each case. Note that computed results for acetone and urea have been added to this plot; their experimental spectra have been reported elsewhere [2]. It is clear from Fig. 9 that the energies of the C 1s and O 1s → $\pi^*_{C=O}$ transitions are determined largely by the electronegativity of the atoms attached to the C=O groups. The π* transition energies of molecules with the same oxidation index are very similar. The main exception to this is the C1s(C=O) → π* transitions of compounds of oxidation index = 2, which appear to have a wider range of energies than for compounds with oxidation indices of 0, 1 and 4. However, the experimental C 1s spectra (Fig. 2) and the computed and experimental O 1s spectra (Fig. 3) do not show this grouping effect, thus, it may be a limitation of the computational accuracy.
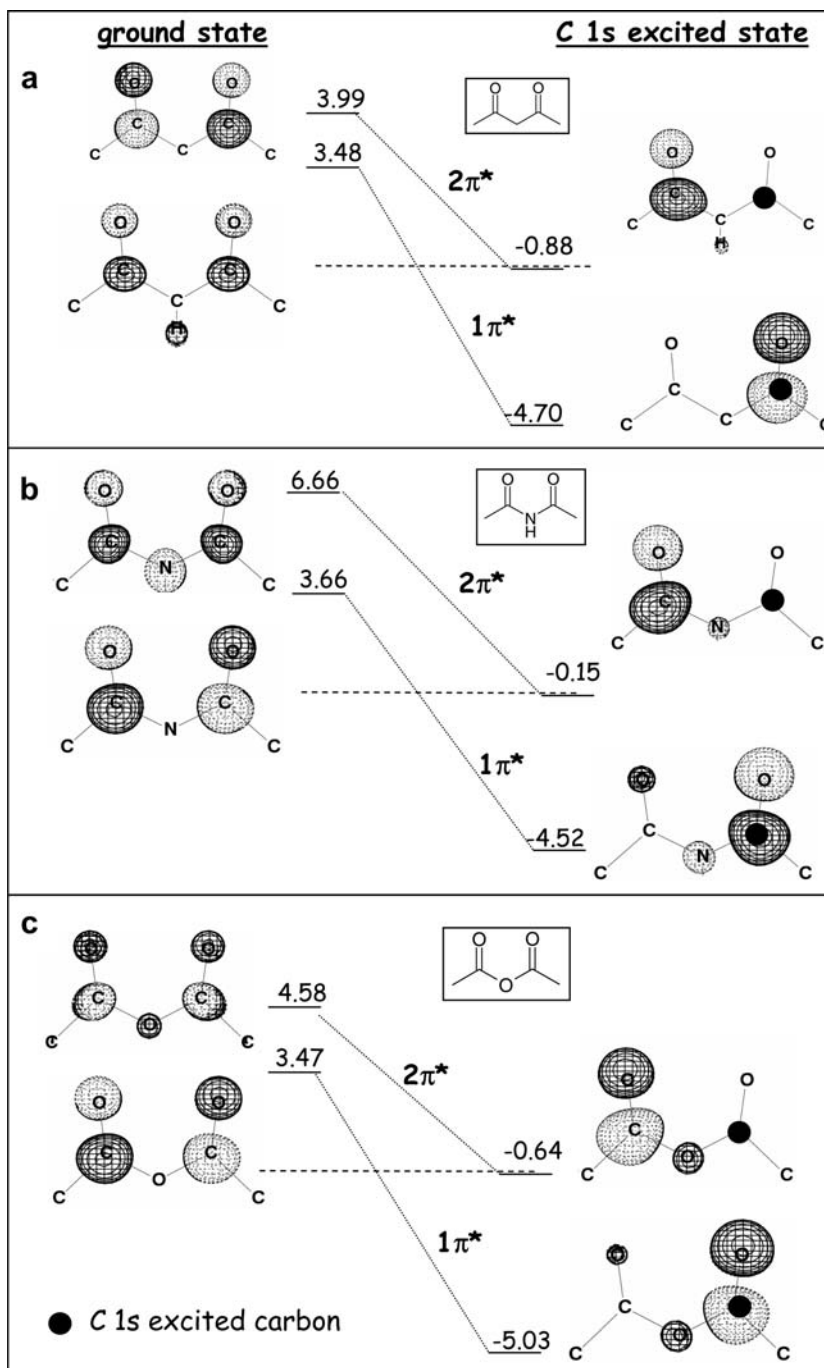
Fig. 5. Energy levels and plots of the $1\pi^*$ ($CO_L + CO_R$) and $2\pi^*$ ($CO_L - CO_R$) molecular orbitals in the ground and C 1s(C=O) excited states for (a) 2,4-pentanedione (A), (b) N-acetylacetamide (B) and (c) acetyl anhydride (D). The black dot indicates the site of the C 1s core hole in each case.

Although one expects the electronic structure of these complex molecules to be influenced by many effects so that a simple oxidation index or electronegativity sum would seem to be an overly simple correlator, in fact the degree of correlation is actually quite remarkable. A related study by Urquhart and Ade of analogous solid state organic compounds showed a very similar linear relationship between the $1s \rightarrow \pi^*_{C=O}$ transition energy and relative oxidation level around the C=O groups for both C 1s and O 1s excitation (see Figs. 3 and 4 of Ref. [18]).

Fig. 10a plots the computed versus the experimental energies for the C 1s $\rightarrow \pi^*_{C=O}$ transition (numerical results are summarized in Table 6). Results for acetone and urea have been added to the plot. Clearly there is an excellent correspondence between the computed and experimental C 1s $\rightarrow \pi^*_{C=O}$ transition energies. The slope of the linear correlation is 0.96(4), with a correlation coefficient of 0.982. The calculations reproduce very well the shifts associated with the changing oxidation state of the carbonyl carbon. However, the absolute agreement is less good,
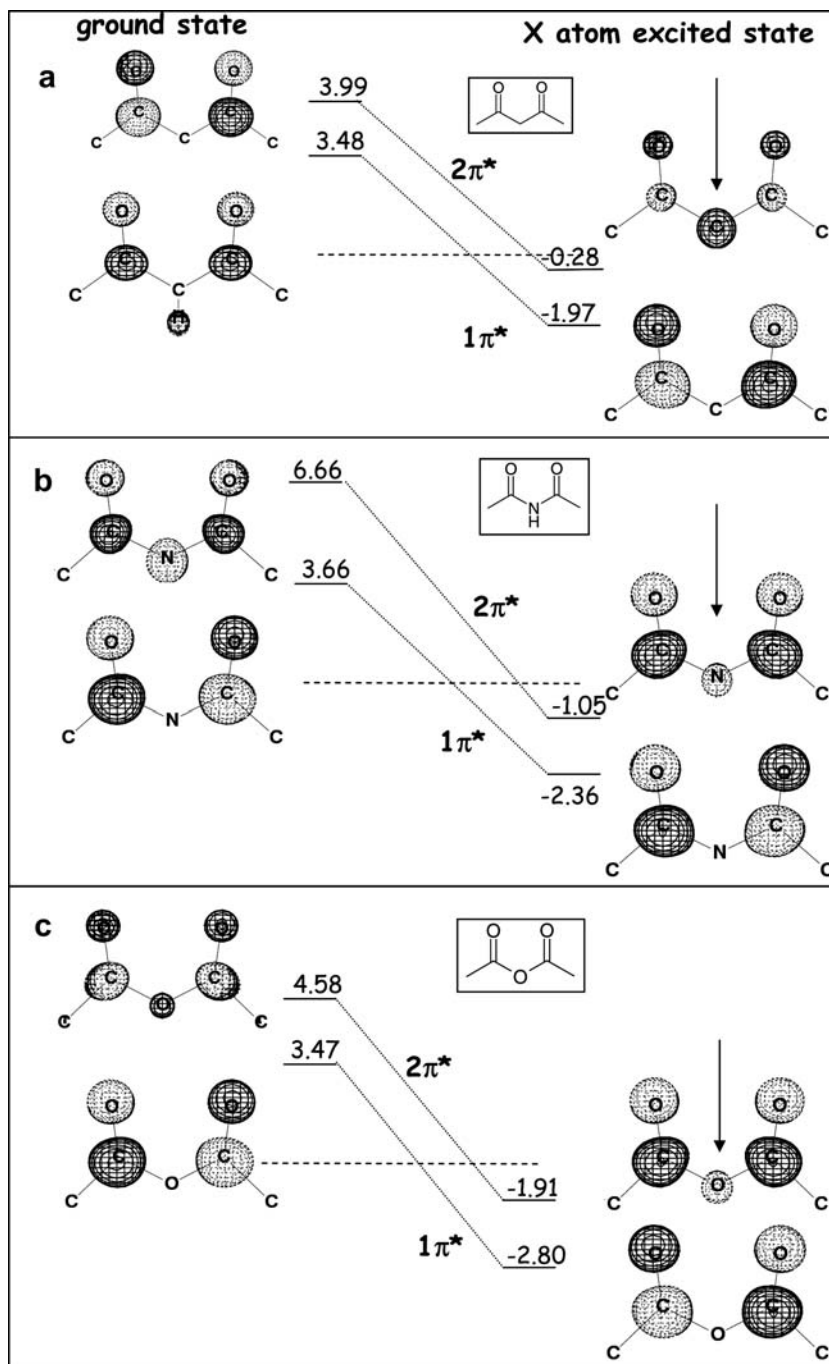
Fig. 6. Energy levels and plots of the $1\pi^*$ ($CO_L + CO_R$) and $2\pi^*$ ($CO_L - CO_R$) molecular orbitals in the ground and X 1s excited states for (a) 2,4-pentanedione (A), (b) N-acetylacetamide (B) and (c) acetyl anhydride (D), where X is the site (CH_2, NH, or O) between the two carbonyls, indicated by the arrow.

due to systematic inaccuracies of GSCF3. In particular, the computed energies are 3.1(1) eV too high relative to the experimental values, as found in many other examples of the use of the GSCF3 program. Urquhart and Ade [18] also found excellent correspondence between experimental and GSCF3 computed C 1s $\rightarrow \pi^*_{C=O}$ and O 1s $\rightarrow \pi^*_{C=O}$ transition energies for the compounds that they studied, after allowing for a similar rigid shift of energy scale.

Fig. 10b plots the experimental transition energies against the computed C 1s(C=O) IP in order to explore the relative contributions of the core and upper π^* levels in establishing the chemical shifts. Results for acetone and urea are also included. While the quality of this correlation is reasonable (slope = 1.05, $r = 0.906$), it is significantly worse than that between the computed and the experimental transition energy. Thus, while a large part of the chemical shift in this series arises from the inductive effect of the heteroatom substituents on the carbonyl carbon, there are also appreciable contributions to the chemical systematics from shifts in the energy of the π^* level.
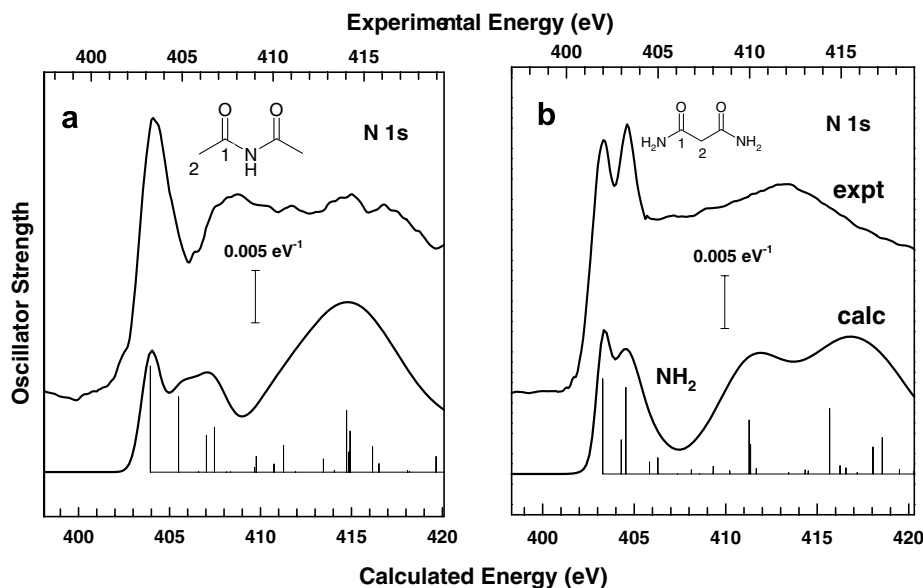
Fig. 7. Computational results for N 1s excitation of (a) *N*-acetylacetamide (B) and (b) malonamide (C), in comparison to the experimental spectra. The computed energy scale is offset by −0.7 eV for B and −1.3 eV for C relative to the experimental scale. See the caption to Fig. 4 for further details.
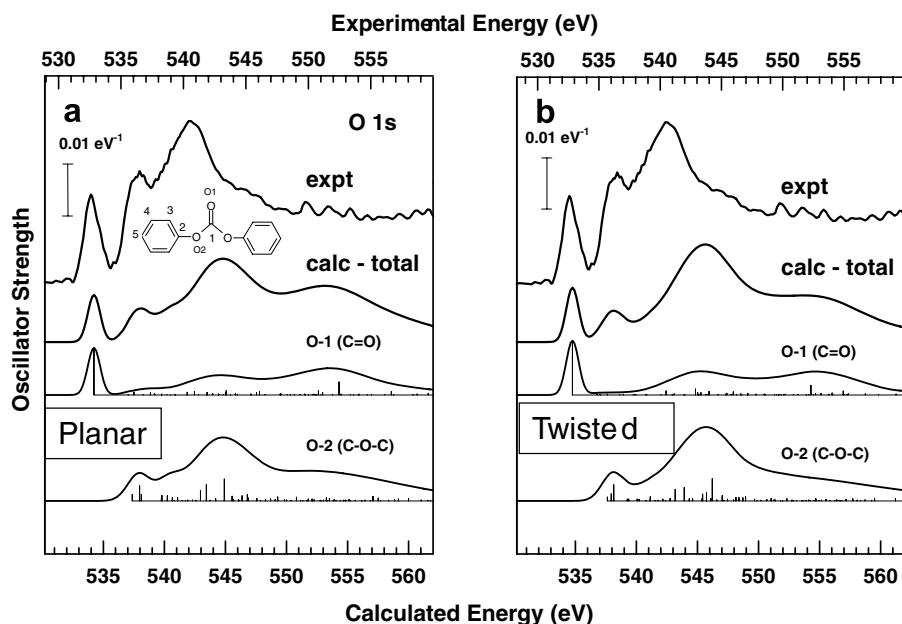

Fig. 8. Computational results for O 1s excitation of diphenylcarbonate (K) in two geometries: (a) planar (the assumed gas phase structure), and (b) twisted (experimental solid state and energy minimized; the twist angle is 55°), in each case compared to the experimental spectrum. The calculated energy scale is offset by −1.5 eV for the planar and −2.1 eV for the twisted geometry, relative to the experimental spectrum.

These can arise from a number of effects, including (i) inductive shifts of the π^* energy, (ii) differences in the core hole stabilization energies, and (iii) perturbations in the π^* level associated with delocalization and mixing of the carbonyl π^* orbital with $2p_z$ orbital components, especially when there is an adjacent NH or O group. Comparison of the computed spectra of the α,γ-dicarbonyl compounds with the corresponding monocarbonyl compounds might be expected to be a way to evaluate the relative importance of these three factors. However, no systematic differences between the two types of compounds can be seen (in

Fig. 10, the monocarbonyl results are plotted as triangles, while the dicarbonyl results are plotted as circles). This may be because the dicarbonyl compounds are effectively behaving like monocarbonyl compounds since the main π^* transitions are localized very much on only one of the two carbonyl groups (see discussion above).

In order to further examine the relative contributions of shifts in the C 1s and $\pi^*_{C=O}$ levels to the chemical systematics, Fig. 11 presents an energy level diagram of the computed C 1s(C=O) IPs and eigenvalues of the $\pi^*_{C=O}$ orbital in the core ionized molecule (taken as the term value for
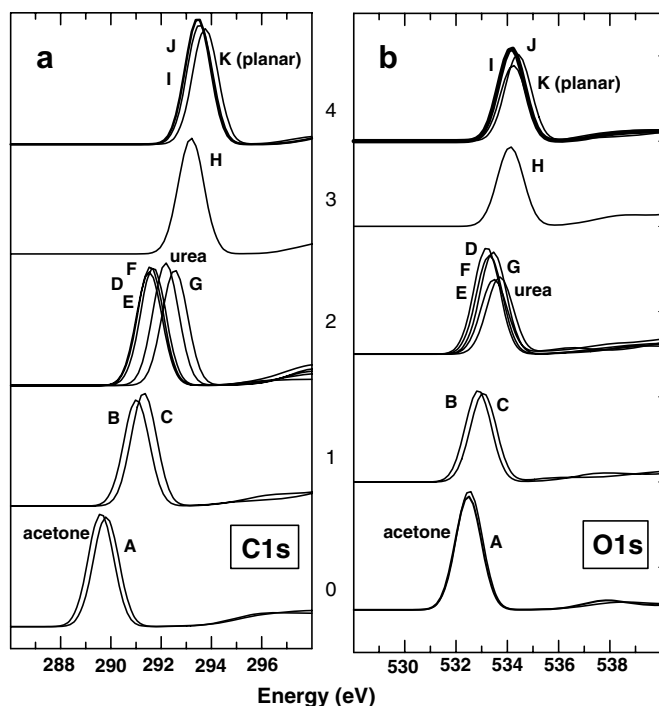
Fig. 9. (a) Plot of the calculated C 1s (C=O) excitation of 2,4-pentanedione (A), acetone, *N*-acetylacetamide (B), malonamide (C), acetyl anhydride (D), dimethyl malonate (E), diethyl malonate (F), 2-imidodicarbonic diamide (G), urea, di-*t*-butyl iminodicarboxylate (H), dimethyldicarbonate (I), dimethoxymethanone (J) and diphenoxymethanone (K). The spectra are grouped according to the oxidation index. (b) Corresponding plot of the O 1s(C=O) excitation of these molecules. The intensities of the two carbonate species are multiplied by 2 to account for the difference in the number of carbonyl groups relative to the α,γ-dicarbonyls.

the C 1s → $\pi^*_{C=O}$ transition, according to the improved virtual orbital approximation). The ordering of the species is set by the computed C 1s(C=O) IP. This plot clearly shows that both the C 1s and the π^* levels are changing. The C 1s IP changes are obviously related systematically to the relative oxidation level number (or sum of electronegativities of X, Y atoms), while the $\pi^*_{C=O}$ MO levels are more sensitive to other, more subtle factors that were mentioned above. For example, even a small amount of extra delocalization of the final state orbital onto an adjacent N atom as compared to a C atom (see Fig. 5) may appreciably change the final $\pi^*_{C=O}$ orbital energy, whereas the core level will be immune to such an effect.

Fig. 12a plots the computed versus the experimental intensities for the C 1s → $\pi^*_{C=O}$ transitions. The experimental values were derived by integration of the $\pi^*_{C=O}$ peak, after subtraction of the underlying background from other transitions. Since this was estimated as a straight line, the uncertainty in the experimental intensities is relatively high. The solid line shown in Fig. 12a is a least squares fit to the data which has an *R* value of 0.862. The quality of the agreement between experiment and the calculated intensities is only fair. This is perhaps not surprising as there is a relatively weak variation in the intensity with carbonyl
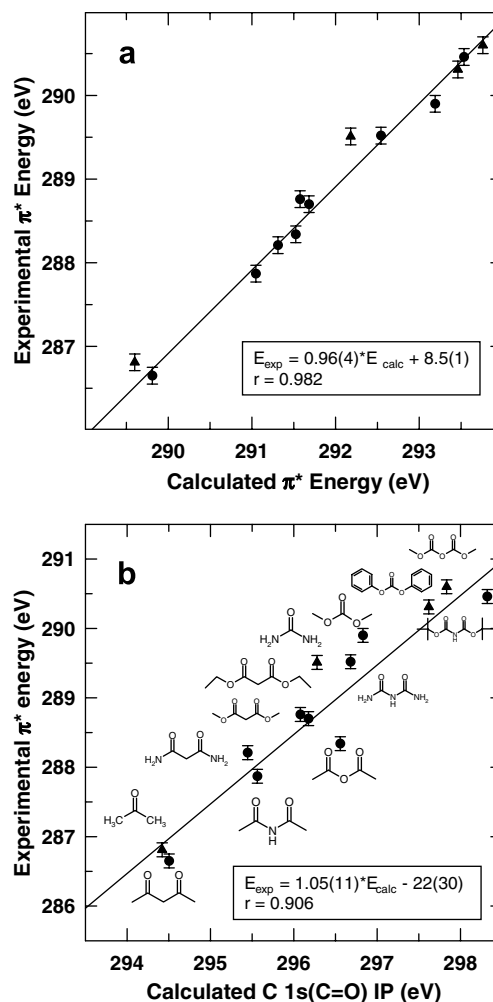

Fig. 10. (a) Plot of the computed versus the experimental C 1s → $\pi^*_{C=O}$ transition energies for all species. (b) Plot of the calculated C1s IP versus the experimental C1s → $\pi^*_{C=O}$ transition energies for all species. Circles are used for the α,γ-dicarbonyl compounds while triangle symbols are used for the monocarbonyl compounds.

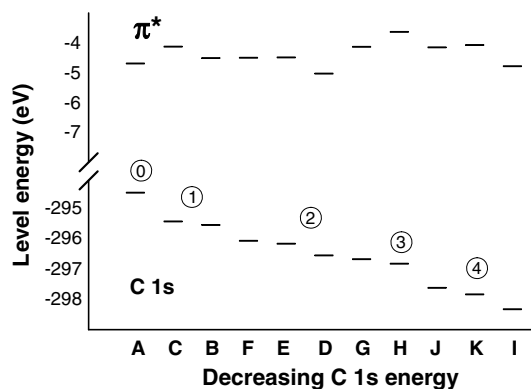Fig. 11. Energy level diagram for the C 1s and $\pi^*_{C=O}$ levels obtained from GSCF3 calculations. The C 1s level is the ΔSCF IP. The $\pi^*_{C=O}$ energy is the eigenvalue of the orbital in the core ionized state (IVO approximation). The species are ordered in increasing C 1s IP. The numbers in circles are the oxidation index. There is no meaning to the spacing between species.
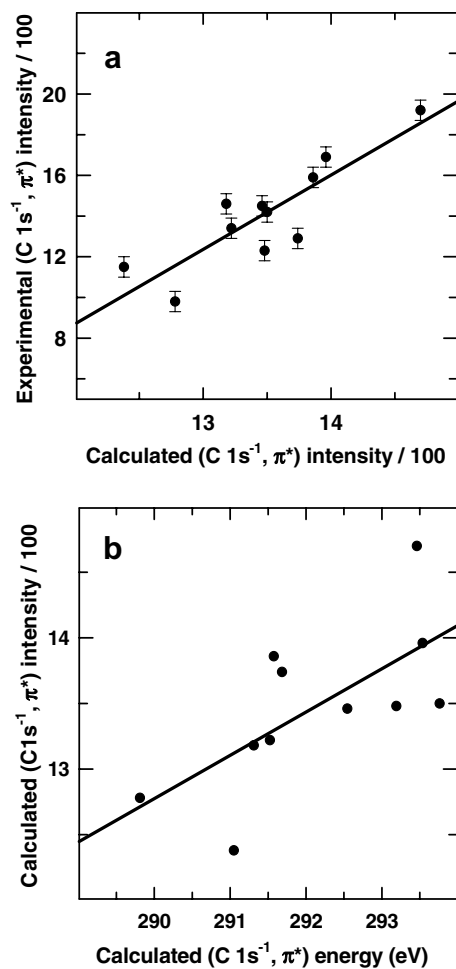
Fig. 12. (a) Plot of the computed versus the experimental intensity for the C1s $\to \pi^*_{C=O}$ transition in all species. The experimental values were obtained by spectral integration after subtraction of a linear background. The values for the two carbonate species have been multiplied by 2 to take into account the different number of carbonyl groups. (b) Plot of the computed energy versus the computed intensity of the C 1s $\to \pi^*$ transition. In both (a) and (b) the solid lines are least squares fits to the data.

oxidation state, and in general the results suffer more from limitations in the calculation of intensities than for transition energies. It is noteworthy that the spread in the calculated intensities is less than 50% of that found experimentally.

Fig. 12b plots the computed energies versus the computed intensities for the C1s $\to \pi^*_{C=O}$ transitions, in order to explore if the oxidation level that drives the C1s $\to \pi^*_{C=O}$ transition energy also influences the transition intensity. The solid line shown in Fig. 12b is a least squares fit to the data which has an R value of 0.674. There is only a small degree of correlation between these properties. This could reflect the intrinsic limitations of the computed intensities, or more probably it suggests that the orbital electron densities which drive spectral intensities are much more subtly influenced by changes in molecular geometry and structure than the spectral transition energies.

5. Summary

The inner shell excitation spectra of two carbonates and nine gas phase α,γ-dicarbonyl compounds have been presented and analyzed with the aid of systematic trends and *ab initio* calculations. The shifts in the 1s $\to \pi^*_{C=O}$ transition energies are found to be systematically related to the relative oxidation of the carbonyl carbon, in agreement with shifts in the inner shell excitation energies for other carbonyl species [18].

Acknowledgements

Appendix A. Supplementary material

Supplementary material includes computational details, plots of all computed spectra in comparison to experimental spectra, and tabulations of the computational results. Supplementary data associated with this article can be found, in the online version, at doi:10.1016/j.chemphys. 2006.10.020.

References

[1] A.P. Hitchcock, J. Electron Spectroscopy Rel. Phenom. 112 (2000) 9.
[2] A.P. Hitchcock, D.C. Mancini, J. Electron Spectrosc. Relat. Phenom. 67 (1994) 1, Updates of this bibliography are available at http://unicorn.mcmaster.ca.
[3] J. Stöhr, NEXAFS Spectroscopy, Springer-Verlag, Berlin, 1992.
[4] I. Nenner, P. Morin, Electronic and Nuclear Relaxation of Core Excited Molecules in VUV and Soft X-ray Photoionization, in: U. Becker, D.A. Shirley (Eds.), Plenum, NY, 1996, p. 291.
[5] J. Kikuma, B. Tonner, J. Electron Spectrosc. Relat. Phenom. 62 (1996) 53.
[6] I. Ouchi, I. Nakai, M. Kamada, S. Tanaka, J. Electron Spectrosc. Relat. Phenom 78 (1996) 363.
[7] M.G. Samant, J. Stöhr, H.R. Brown, T.P. Russell, J.M. Sands, S.K. Kumar, Macromolecules 29 (1996) 8334.
[8] J. Kirz, C. Jacobsen, M. Howells, Q. Rev. Biophys 28 (1995) 33.
[9] H. Ade, A.P. Smith, H. Zhang, G.R. Zhuang, J. Kirz, E. Rightor, A. Hitchcock, J. Electron Spectrosc. Relat. Phenom. 84 (1997) 53.
[10] H. Ade, Trends Polym. Sci 5 (1997) 58.
[11] H. Ade, X-ray Spectromicroscopy in Experimental Methods In The Physical Sciences 32, in: J.A.R. Samson, D.L. Ederer (Eds.), Academic Press, NY, 1998, pp. 225–261.
[12] H. Ade, S.G. Urquhart, NEXAFS Spectroscopy and Microscopy of Natural and Synthetic Polymers in Chemical Applications of Synchrotron Radiation, in: T.K. Sham (Ed.), World Scientific, Singapore, 2000.
[13] R.F. Egerton, Electron Energy Loss Spectroscopy in the Electron Microscope, Plenum Press, New York, 1996.
[14] L.C. Sawyer, D.T. Grubb, Polymer Microscopy, Chapman and Hall, NY, 1987.

[15] N. Kosugi, H. Kuroda, Chem. Phys. Lett 74 (1980) 490.

[16] N. Kosugi, Theor. Chim. Acta 72 (1987) 149.

[17] L. Pauling, J. Am. Chem. Soc. 54 (1932) 3570.

[18] S.G. Urquhart, H. Ade, J. Phys. Chem. B 106 (2002) 8531.

[19] A.P. Hitchcock, S.G. Urquhart, E.G. Rightor, J. Phys. Chem. 96 (1992) 8736.

[20] E.G. Rightor, A.P. Hitchcock, H. Ade, R.D. Leapman, S.G. Urquhart, A.P. Smith, G. Mitchell, D. Fisher, H.J. Shin, T. Warwick, J. Phys. Chem. B 101 (1997) 1950.

[21] S.G. Urquhart, A.P. Hitchcock, A.P. Smith, H. Ade, E.G. Rightor, J. Phys. Chem. B 101 (1997) 2267.

[22] S.G. Urquhart, A.P. Hitchcock, R.D. Leapman, R.D. Priester, E.G. Rightor, J. Polym. Sci. B: Polym. Phys. 33 (1995) 1593.

[23] S.G. Urquhart, A.P. Hitchcock, R.D. Priester, E.G. Rightor, J. Polym. Sci. B: Polym. Phys. 33 (1995) 1603.

[24] R.N.S. Sodhi, C.E. Brion, J. Electron Spectrosc. Relat. Phenom. 34 (1984) 363.

[25] Y. Ma, C.T. Chen, G. Meigs, K. Randall, F. Sette, Phys. Rev. A 44 (1991) 1848.

[26] I. Ishii, A.P. Hitchcock, J. Electron Spectrosc. 46 (1987) 55.

[27] N. Kosugi, E. Shigemasa, A. Yagishita, Chem Phys. Lett. 190 (1992) 481.

[28] N. Kosugi, J. Adachi, E. Shigemasa, A. Yagishita, J. Chem. Phys. 97 (1992) 8842.

[29] W.J. Hunt, W.A.I. Goddard, Chemical Physics Letters 3 (1969) 414.

[30] L. Triguero, L.G.M. Pettersson, H. Agren, Phys. Rev. B 58 (1998) 8097.

[31] W. Domcke, L.S. Cederbaum, Chem. Phys. 25 (1977) 189.

[32] A.P. Hitchcock, S.G. Urquhart, A.T. Wen, A.L.D. Kilcoyne, T. Tyliszczak, E. Rühl, N. Kosugi, J.D. Bozek, J.T. Spencer, D.N. McIlroy, P.A. Dowben, J. Phys. Chem. B 101 (1997) 2267.

[33] F.X. Gadea, H. Koppel, J. Schirmer, L.S. Cederbaum, K.J. Randall, A.M. Bradshaw, Y. Ma, F. Sette, C.T. Chen, Phys. Rev. Lett. 66 (1991) 883.

[34] L.S. Cederbaum, J. Chem. Phys. 103 (1999) 562.

[35] M.W. Schmidt, K.K. Baldridge, J.A. Boatz, S.T. Elbert, M.S. Gordon, J.J. Jensen, S. Koseki, N. Matsunaga, K.A. Nguyen, S. Su, T.L. Windus, M. Dupuis, J.A. Montgomery, J. Comput. Chem. 14 (1993) 1347.

[36] SPARTAN molecular modeling package, Wavefunction Inc.

[37] S. Huzinaga, J. Andzelm, M. Klobokowski, E. Radzio-Andzelm, Y. Sasaki, H. Tatewaki, Gaussian Basis Sets for Molecular Calculations, Elsevier, Amsterdam, 1984.

[38] A.T. Wen, E. Rühl, A.P. Hitchcock, Organometallics 11 (1992) 2559.

[39] C.C. Turci, S.G. Urquhart, A.P. Hitchcock, Can. J. Chem. 74 (1996) 851.

[40] G. Cooper, K.H. Sze, C.E. Brion, J. Am. Chem. Soc. 111 (1989) 5051.

[41] G. Cooper, K.H. Sze, C.E. Brion, J. Am. Chem. Soc. 112 (1990) 4221.

[42] C.C. Turci, S.G. Urquhart, A.P. Hitchcock, Can. J. Chem. 74 (1996) 851.

[43] J.A. King Jr., G.L. Bryant, Acta Crystallogr. C 49 (1993) 550.

[44] M.B. Robin, I. Ishii, R. McLaren, A.P. Hitchcock, J. Electron Spectrosc. 47 (1988) 53.

[45] S.G. Urquhart, A.P. Hitchcock, R.D. Priester, E.G. Rightor, J. Polym. Sci. B: Polym. Phys. 33 (1995) 1603.